Assignment of solid-state ^{13}C and ^{1}H NMR spectra of paramagnetic Ni(II) acetylacetonate complexes aided by first-principles computations

Syed Awais Rouf[1,#], Vibe Boel Jakobsen[2,3#], Jiří Mareš[1], Nicholai Daugaard Jensen[2], Christine McKenzie[2], Juha Vaara[1], and Ulla Gro Nielsen[2,*]

# These authors contributed equally.

[1] NMR Research Unit, University of Oulu, P.O. BOX 3000, FIN-90014 Oulu, Finland

[2] Department of Physics, Chemistry, and Pharmacy, University of Southern Denmark, 5230 Odense M, Denmark

[3]Current address: School of Chemistry, University College Dublin, Belfield, Dublin 4, Ireland

*Corresponding author: email: ugn@sdu.dk phone: +45 6550 4401

Abstract:

Recent advances in computational methodology allowed for first-principles calculations of the nuclear shielding tensor for a series of paramagnetic nickel(II) acetylacetonate complexes, $[Ni(acac)_2L_2]$ with L = H_2O, D_2O, NH_3, ND_3, and PMe_2Ph have provided detailed insight into the origin of the paramagnetic contributions to the total shift tensor. This was employed for the assignment of the solid-state $^{1,2}H$ and ^{13}C MAS NMR spectra of these compounds. The two major contributions to the isotropic shifts are by orbital (diamagnetic-like) and contact mechanism. The orbital shielding, contact, as well as dipolar terms all contribute to the anisotropic component. The calculations suggest reassignment of the ^{13}C methyl and carbonyl resonances in the acac ligand [*Inorg. Chem.* **53**, *2014*, 399] leading to isotropic paramagnetic shifts of $\delta(^{13}C) \approx$ 800-1100 ppm and ≈ 180-300 ppm for ^{13}C for the methyl and carbonyl carbons located three and two bonds away from the paramagnetic Ni(II) ion, respectively. Assignment using three different empirical correlations, *i.e.*, paramagnetic shifts, shift anisotropy, and relaxation (T_1) were ambiguous, however the latter two support the computational results. Thus, solid-state NMR spectroscopy in combination with modern quantum-chemical calculations of paramagnetic shifts constitutes a promising tool for structural investigations of metal complexes and materials.

Keywords: Ni(II), acetyl acetonate, solid state NMR, paramagnetic shift, first-principles calculation, paramagnetic NMR

1. Introduction

Transition metal-organic compounds find widespread application in catalysis, energy storage and conversion, as well as selective capture of molecules or ions. It is the flexible oxidation states of the transition metal(s) that are essential for many of these functions in a vast number of chemical processes ranging from the selectivity of metallo-enzymes in biological processes and industrial catalysis, to the binding and degradation of pollutants in the environment. These materials are often part of complex systems without long-range order, thus single crystals suitable for structure determination by X-ray diffraction may be difficult to obtain. Other experimental techniques with atomic-level resolution for solid state materials are needed to link the function to the chemical structure. Solid-state NMR spectroscopy (SSNMR) combined with first-principles calculations have proven invaluable for the interpretation and prediction of experimental data in studies of complex metal-organic and inorganic materials. Especially the density functional theory-based methods (DFT) pioneered by Pickard, Mauri and co-workers[1-3], are widely used, DFT methods however are mainly successful for diamagnetic systems[4, 5].

Recent advances in NMR methodology have facilitated the acquisition of high-resolution SSNMR spectra by fast magic-angle spinning (MAS)[6-9] and NMR pulse sequences for paramagnetic systems[10-15]. However, the analysis of paramagnetic NMR (pNMR) spectra is much more complicated than for their diamagnetic analogues due to the large magnetic moments of the unpaired electrons. Furthermore, efficient and accurate quantum-chemical models for paramagnetic systems have only recently become available[16-25]. Thus, the analysis of SSNMR spectra of paramagnetic samples has mainly relied on simple empirical and/or classical models (Figure 1). In particular, the paramagnetic hyperfine contribution ("Fermi contact shift") to the isotropic shifts ("paramagnetic shifts") has been popular due to its simplicity, with applications to, e.g., battery materials[26, 27], iron soil minerals[26-29], and recently to metal-organic complexes [30-37].

Recent studies show that such simple rules fail for metal-organic frameworks (MOFs), as demonstrated by Dawson et al.[38] in the analysis of ^{13}C MAS NMR spectra of two Cu(II)-containing MOFs[38]. Kong *et al.* recently investigated a series of metal-organic complexes including [V(III)$(acac)_3$] and [Mn(III)$(acac)_3$] using ^{17}O SSNMR in combination with conventional DFT methods, but were unable to unambiguously assign the ^{17}O resonances in the spectra of these two complexes[37].

In addition to the Fermi contact interaction, the paramagnetic dipolar interaction may be used for the determination of distances to the paramagnetic center in metal-organic systems[10, 39-41]. This requires a precise determination of the anisotropies by analysis of the spinning sideband pattern, which can be difficult due to the overlap of spinning side bands, ssbs from different sites, and the large spinning speeds needed, which partially average the dipolar interaction. From an experimental point of view, the isotropic shifts, which can be measured directly, are preferred for assignment. Finally, $\{^{1}H,^{13}C\}$-correlation SSNMR experiments and relaxation measurements in combination with fast MAS, probe the bonding connectivities and distances to the paramagnetic center, respectively[6-8]. However, the combination of fast MAS, short relaxation times and large chemical shift range, *i.e.*, inefficient polarization transfer render this approach experimentally quite demanding[8, 13, 14, 38].

Computation of pNMR parameters requires that the theoretical framework of standard NMR is expanded to include the strong interaction between the magnetic moments of the unpaired electron(s) with the magnetic field. The zero-field splitting (ZFS) represents a challenge for the NMR parameters in paramagnetic systems with two or more unpaired electrons, *i.e.*, as total electron spin (S) of one or more ($S \geq 1$). For $S \geq 1$, ZFS lifts the degeneracy of the ground-state multiplet resulting in $(2S+1)$ states separated often by only a small energy difference, which is accompanied by a more complex pattern of hyperfine shielding interactions[16], than assumed in

classical models. In particular, the leading-order dipolar hyperfine coupling now contributes to the isotropic shifts due to the ZFS[16], whereas the contact coupling influences the shielding anisotropy. Furthermore, a thermal average over both the ground multiplet and thermally occupied states above the ground multiplet must be included in the calculation. The formal derivation for the pNMR nuclear shielding expression as a quantum-statistical expectation value was introduced in the classic paper by Kurland and McGarvey[42]. Subsequently, Soncini and Van den Heuvel[18] presented the correct formulation for the ZFS within the $(2S+1)$–dimensional ground multiplet using the standard electron paramagnetic resonance (EPR) parameters. References. [16, 17, 21] include a detailed analysis of the shielding contributions in terms of the physical mechanisms underlying the hyperfine coupling tensor as well as the *g*-tensor, which parameterizes the Zeeman interaction between the unpaired electrons and the external magnetic field. The terms include $\boldsymbol{\sigma}_{\mathrm{orb}}$ for orbital shielding (often called chemical shielding in the SSNMR literature) and a total of nine "hyperfine" contributions (Table 1 and Figure 1).

Open-shell systems are inherently multiconfigurational, which often results in failure of DFT methods for calculations of EPR parameters, particularly the ZFS-tensors[43]. Therefore reliable computations may only be obtained at higher, *ab initio* levels that can take into account for the multiconfigurational nature of the electronic structure of metal-organic systems. A useful level of agreement with the experimental pNMR shifts can be reached by a combination of the complete-active space self-consistent field (CASSCF)[44] and *N*-electron valence-state perturbation theory (NEVPT2, see ref. [45] and references therein) calculation of the critical interactions (ZFS and the *g*-tensor)[17], as also demonstrated in the current work. In contrast, much of the computational work on pNMR shifts is still based on the phenomenological contact and dipolar shifts[46], which disregards the ZFS and thereby provides an incomplete description. However, a number of studies using modern methods have recently been reported, which give a more complete description[17, 19,

20, 47, 48].

The situation in the molecular pNMR shift theory has been reviewed in References [47, 49, 50]. It is noteworthy that, in contrast to the situation in the SSNMR of diamagnetic systems for which periodic DFT methods[4] are routinely used[51], so far no periodic implementation of the modern first-principles pNMR theory with ZFS exist. Currently, modeling is therefore restricted to molecular quantum-chemistry codes.

Our study reports a combined, ^{1,2}H and ^{13}C MAS NMR and modern quantum-chemical study of [Ni(II)(acac)$_2$L$_2$] for L = H_2O, D_2O, NH_3, ND_3, and PMe_2Ph (Figure 2), for which the ^{13}C NMR chemical shift tensors were reported earlier (except for L = ND_3) and assigned using empirical paramagnetic shift rules[31]. Quantum-chemical calculations provide a valuable asset in verifying the identity of the pNMR signals. Thus, additional SSNMR experiments were performed on these complexes to resolve this ambiguity for [Ni(II)(acac)$_2$L$_2$] for L = H_2O, D_2O, NH_3, and ND_3. These [Ni(II)(acac)$_2$L$_2$] complexes constitute excellent model systems to compare the different computational approaches. Moreover, [Ni(II)(acac)$_2$(PMe$_2$Ph)$_2$], which contains a more complex, organic ligand, allows us to test computationally the assignment based on isotropic shifts only.

2. Methods and Materials

2.1 Synthesis: Polycrystalline [Ni(II)(acac)$_2$], [Ni(II)(acac)$_2$(H_2O)$_2$]H_2O, [Ni(II)(acac)$_2$(D_2O)$_2$]D_2O and [Ni(II)(acac)$_2$(NH_3)$_2$] were synthesized following the procedures in Ref [31]. Deuterated ammonia (25% solution in D_2O) was obtained from Cambridge Isotope Laboratories.

Two methods were used for preparation of [Ni(II)(acac)$_2$(ND_3)$_2$]. Method A: Solid [Ni(II)(acac)$_2$] was exposed to gaseous deuterated ammonia generated by adding drops of D_2O to solid lithium nitride in a closed vessel. The color of the solid changed from pale green to pale blue over 30 mins.

Method B: [Ni(II)(acac)$_2$] (0.65 g, 2.5 mmol) was dissolved in ethylacetate (30mL) with heating. The mixture, in an open vial, was placed inside a larger container containing 4 mL of 25 % ND_3 in D_2O and sealed to allow ND_3 vapor diffusion into the vial. Within minutes microcrystalline pale blue [Ni(II)(acac)$_2$(ND_3)$_2$] was deposited. This was collected by suction filtration (0.71g, 94%).

PXRD confirms that both samples of [Ni(acac)$_2$(ND_3)$_2$] are isostructural to [Ni(acac)$_2$(NH_3)$_2$] and all reflections could be assigned to this phase (Figure S1). Anal. Calcd. for the sample prepared by method A shows that uptake ammonia is not complete: $C_{10}H_{12}D_8NiN_2O_4$ (MW = 298.8 with fully deuterated acac methine and ammonia ligands): C, 40.17; H/D, 9.43; N, 9.37. Found: C, 38.94(7); H/D, 6.44(1); N, 6.72(1). The sample prepared by Method B was pure according to ^{2}H MAS NMR and ^{13}C MAS NMR (δ(^{13}C) = 118(2) and 199(1) ppm) matching our earlier reported data for the [Ni(II)(acac)$_2$(NH_3)$_2$] complex[31]. $C_{10}H_{12}D_8NiN_2O_4$ (MW = 298.8 with fully deuterated acac methine and ammonia ligands): C, 40.17; H/D, 9.43; N, 9.37. Found: C, 40.66(3); H/D, 6.70(15); N, 9.46(6). The C/N ratios, which are independent of the level of deuteration, are 4.28 and 4.29(4) for the calculated and experimental values, respectively for sample B.

2.2 Solid-state NMR spectroscopy: ^{1}H, ^{2}H, and ^{13}C single-pulse and inversion recovery experiments were performed at 11.7 T (500 MHz (^{1}H), 76.7 MHz (^{2}H) and 125.7 (^{13}C)) on an INOVA 500 MHz NMR spectrometer using a 3.2 mm HX MAS NMR probe and 18-22 kHz MAS. Two sets of inversion recovery experiments with the carrier at about 900 and 200 ppm were recorded to ensure complete inversion of the magnetization. Additional ^{1}H, ^{2}H, and ^{13}C, MAS NMR spectra were recorded at 14.1 T using a 3.2 mm HXY probe on an Agilent 600 MHz spectrometer with 599.8 92.05, and 150.8 MHz Larmor frequencies for ^{1}H, ^{2}H and ^{13}C, respectively. ^{13}C and ^{2}H MAS NMR spectra were recorded using a rotor-synchronized Hahn echo sequence (90-τ-180-τ, τ = 1 rotor

period). Spectra were recorded at ambient temperature and only minor changes (≈ 1 ppm) in the isotropic shifts were observed by changing the spinning speed (frictional heating).

3. Calculations

3.1 Computational Details

We used the theory of Kurland & McGarvey[42] and Soncini & van den Heuvel[18, 42] combined with our computational methodology and analyses reported elsewhere[17, 21]. The necessary quantities were calculated by two different quantum-chemical packages. $\boldsymbol{\sigma}_{orb}$ (the chemical shielding (CSA) tensor) was obtained with GAUSSIAN 09 (G09)[52] and the *g*-tensor (***g***), the ZFS tensor (***D***), and the hyperfine coupling (HFC) tensor (***A***) were calculated with ORCA[53]. The computations for $\boldsymbol{\sigma}_{orb}$ and ***A*** were performed at the density functional theory (DFT) level with the generalized gradient approximation-type functional PBE[54, 55] and the hybrid functional (with 25% exact-exchange admixture) PBE0[56], while the computations of ***g*** and ***D*** were done with *ab initio* wave function theory at the CASSCF and NEVPT2 levels. The notation used throughout the article for these calculations is CASSCF/DFT(PBE) or NEVPT2/DFT(PBE) denoting combined methods where either CASSCF or NEVPT2 was used for ***g*** and ***D*** and PBE was used for ***A***. Similarly, in CASSCF/DFT(PBE0) or NEVPT2/DFT(PBE0) calculations, PBE0 was employed for ***A.*** The active space in our state-average CASSCF wave functions, which also were underlying the NEVPT2 calculations, consisted of the eight metal *d*-electrons in the five Ni(3*d*) orbitals. All 10 triplet and 15 singlet states allowed by the CAS(8,5) calculation were included.

Three different kinds of geometries were used in the computations: besides the experimental X-ray structures[31], for [Ni(II)$(acac)_2(H_2O)_2$] and [Ni(II)$(acac)_2(NH_3)_2$] depicted in Figure 2, we additionally used both fully optimized (meaning that the positions of all the atoms were optimized)

structure and 'hydrogen-optimized' structure. In the latter, the positions of only the hydrogen atoms were optimized, while the heavier atoms retained their X-ray positions. The optimizations were performed using the Turbomole program[57] at the B3LYP[58-60]/def2-TZVP[61, 62] level of theory. For [Ni(II)$(acac)_2(NH_3)_2$], the geometry optimization was also carried with a dispersion-corrected PBE0[56] level of theory (PBE0-D3[63]) for the purpose of comparison with data calculated with B3LYP.

The all-electron def2-SVP, def2-TZVP and def2-QZVPP[61, 62] basis sets were applied for all the atoms in the ***A*** tensor calculations. In contrast, locally dense basis sets (LDBS)[64-66] were used for ***g*** and ***D***, meaning that, for the metal ion and the atoms directly bonded to it, we used better basis sets such as TZVP or QZVPP, while for the more distant atoms we used the smaller SVP basis. The purpose of adopting LDBS was to reduce the computational cost; the spin density distribution that gives rise to ***g*** and ***D*** is localized in the immediate neighborhood of the metal ion. Therefore, LDBS (denoted as TZVP* or QZVPP*) performs equally well as, and is less expensive than calculation with fully balanced (FB) TZVP or QZVPP basis set. However, the HFC calculations were performed with the FB basis, because of the high sensitivity of ***A*** of the NMR centers to the flexibility of the basis set. The corresponding representations for the basis sets are SVP/SVP, TZVP*/TZVP, and QZVPP*/QZVPP, where the first basis sets specified was used for ***g*** and ***D***, and the second set was used for ***A***.

The chemical shifts are reported with respect to tetramethylsilane (TMS), a diamagnetic reference molecule. The ^{1}H and ^{13}C shielding constants for TMS were calculated with G09 using DFT with the same exchange-correlation functionals and FB basis sets, as used for the present Ni(II) complexes. All the calculated paramagnetic shifts are reported at the temperature of 298 K. The calculated shieldings are averaged within the experimentally equivalent group of nuclei except for [Ni(II)$(acac)_2(H_2O)_2]H_2O$, for which crystallographically inequivalent ^{13}C can be identified. Here

the individual ^{1}H and ^{13}C data are reported from our best calculations using the X-ray positions except for hydrogen, for which geometry optimization was performed. All calculations were carried out *in vacuo*; no solid-state effects such as intermolecular hydrogen bonds and solvent molecules were included. This means that also crystallographic water molecules were omitted.

3.2 Definitions and conventions for NMR parameters

The analysis of experimental SSNMR spectra for I = ½ nuclei in paramagnetic systems allows for a direct determination of the principal components of the total shielding (shift) tensor. However, comparison of the experimental and computational approaches is complicated by the different terminology used by the NMR and computational communities. Thus, we establish the link between these below.

Three factors contribute to the isotropic shift, δ:

$$\delta = \delta_{orb} + \delta_{con} + \delta_{pc} \qquad (2)$$

δ_{orb} reflects the shielding of the nucleus by the electrons and it is the only observable isotropic component in diamagnetic systems. From an experimental NMR point of view, two factors may contribute to the paramagnetic shift: the contact shift (δ_{con}) and the pseudocontact shifts (δ_{pc}). δ_{con} is caused by unpaired electron spin density at the NMR nucleus mediated through the chemical bonds similar to the scalar J-coupling, and is often referred to as the Fermi contact shift (δ_{fc}). δ_{pc} arises due to the dipolar HFC interaction and depends on the distance between the paramagnetic center(s) and NMR nucleus[39].

The anisotropic components, *i.e.*, the total anisotropy ($d = \delta_{zz} - \delta$) and the asymmetry parameter $\eta_d = (\delta_{xx} - \delta_{yy}) / d$, generally contain contributions from both the CSA ("orbital" term) and the paramagnetic dipolar interaction. For which the following convention is used: $|\delta_{zz} - \delta| \geq |\delta_{xx} - \delta| \geq$

$|\delta_{yy} - \delta|$. The CSA may experimentally be estimated based on the chemical shift parameters for an isostructural, diamagnetic compound, and the relative size of the two contributions obtained. Alternatively, extensive variable temperature experiments of the paramagnetic compound are required[40] in contrast to quadrupole and paramagnetic dipole interactions, which can be separated by 2D NMR[10-12]. The experimentally determined paramagnetic dipole tensor has successfully been analyzed using a classical dipole approximation combined with experimentally determined properties including spin, susceptibility, *g*-tensor, crystal structure, and temperature[8, 10, 40, 67]. However, delocalization of the electron density, as is often observed, requires modification of the classical dipolar model[10, 39]. The Fermi contact (hyperfine) interaction directly reflects the spin delocalization and cannot be modelled by a classical approach. The Kurland-McGarvey[42] and Soncini –van der Heuvel [18] theories, analyzed as in Reference [21] indicates that a total of ten terms may contribute to the total shift tensor (Table 1), three of which contain the dipolar hyperfine interaction (terms 2, 7, and 9 in Table 1) and which may be used in a classical point-dipole approximation for long-range pseudocontact shifts, see References [17, 49] for a detailed discussion of the various mechanisms.

4. Results and discussion

First we discuss the experimental ^{13}C NMR data obtained for $[Ni(acac)_2(ND_3)_2]$, a representative example of the $[Ni(acac)_2L_2]$ complexes, and then compare the different experimental and computational approaches for the assignment of ^{13}C SSNMR spectra of paramagnetic complexes. Following the assignment of the simple complexes (L = H_2O, D_2O, NH_3, and ND_3), our approach is employed for the assignment of the ^{13}C resonances in $[Ni(acac)_2(PMe_2Ph)_2]$, which contains a total of ten crystallographically inequivalent carbon atoms. Finally, assignment of ^{1,2}H NMR data based on the computational results is presented.

4.1 Assignment of ^{13}C MAS NMR spectra of simple [Ni(acac)$_2$L$_2$] complexes using empirical correlations

The experimental ^{13}C MAS NMR spectrum of *trans*-[Ni(acac)$_2$(ND$_3$)$_2$] (Sample B) in Figure 3 is expected to contain three different ^{13}C resonances: a methyl (CH_3), a methine (CH), and a carbonyl (C=O), based on the crystal structure of *trans*-[Ni(acac)$_2$(ND$_3$)$_2$] [31]. Three sets of resonances from *trans*-[Ni(acac)$_2$(ND$_3$)$_2$] are indeed observed at $\delta(^{13}C)$ = 118(2), 198(2), and 885(10) ppm, *c.f.*, Table 2 in excellent agreement with earlier reported data for the non-deuterated analogue[31]. Furthermore, weaker resonances are observed at $\delta(^{13}C)$ = 126(2) and 178(5) ppm as well as two or more resonances in the regions ≈165-185, 285-300, and ≈ 940(20) ppm, which we propose to be *trans*-[Ni(II)(acac)$_2$(H$_2$O)(ND$_3$)], *vide infra*. Analysis of the spinning sideband manifold allowed for precise determination of the total anisotropy (*d*) for the two sites with $\delta(^{13}C)$ = 118(1) and 198(2) ppm, whereas the site with $\delta(^{13}C)$ = 885(10) ppm a larger linewidth and only a single spinning sideband is observed, implying a small anisotropy. Table 2 summarizes these results along with the T_1's for *trans*-[Ni(II)(acac)$_2$L$_2$] with L = H$_2$O, D$_2$O, and NH$_3$. These data illustrate the three different methods of spectral assignment: paramagnetic shifts, shift anisotropy, and relaxation measurements (T_1).

Using the large paramagnetic shift (> 700 ppm), the site with $\delta(^{13}C)$ = 885(10) is assigned to the carbonyl group (C=O), which is directly coordinated to Ni(II). The resonances at $\delta(^{13}C)$ = 118(2) and 198(2) ppm are assigned to the methine and methyl groups by inspection of the single crystal X-ray structure and comparison with other simple *trans*-[Ni(acac)$_2$L$_2$]-complexes, as described in detail in Ref. [31].

Based on the distance to Ni(II), the paramagnetic center, the magnitude of the total anisotropy (*d*) is expected to be $d(CH_3) < d(CH) < d(CO)$. Hence, the resonances in the regions $\delta(^{13}C)$ = 118(2),

198(2) and 988(10) ppm should be assigned to CH, C=O, and CH_3, respectively, *c.f.*, Table 2. Thus, the assignment of the CH_3 and C=O resonances are interchanged with respect to the assignment based on the isotropic paramagnetic shifts (*vide supra*).

The third assignment approach uses the longitudinal relaxation times (T_1, Table 2) under the assumption of no delocalization of the unpaired electron, as T_1 is proportional to r^{-6}[8]. The C=O, CH, and CH_3 groups are 2.95, 3.307, and 4.33 Å from the paramagnetic Ni(II) center, respectively[31]. The site with the shortest T_1 should be the C=O group, *i.e.*, $\delta(^{13}C)$ = 199 ppm, whereas 119 and 883 ppm are assigned to CH and CH_3, respectively, in agreement with the anisotropy (*vide supra*). However, the use of T_1's is not possible for $[Ni(acac)_2(H_2O)_2]\cdot H_2O$, as the experimentally determined T_1 values are identical within the experimental uncertainty for the four signals with $\delta \approx 180 - 300$ ppm and the two broad resonances with $\delta \approx 800$ and 900 ppm. Furthermore, the computational results show significant delocalization of the unpaired electron spin density (Sec. 4.2). Thus, the three different empirical approaches give contradicting results for the assignment of the ^{13}C resonances. To resolve this ambiguity we turn to the computational results.

4.2 Computationally assisted assignment of the [Ni(II)(acac)$_2$L$_2$] complexes using ^{1}H and ^{13}C shifts

Trans-$[Ni(acac)_2(NH_3)_2]$ was used for the calibration of the computational model, as the structure does not contain any co-crystallized solvent molecules[31]. A complete discussion of the basis-set and electron correlation effects, as well as the influence of the choices of the DFT functional and structure is given in the Supporting Information. Three different structural models were investigated encompassing 1) The reported crystal structure[31] and two structures with geometry optimization: i) hydrogen atoms only and ii) all atomic positions. The isotropic ^{1}H and ^{13}C NMR shifts obtained from these three models are reported in Table 3 for calculations at the NEVPT2/PBE0 (NEVPT2 *ab initio* method for the *g*- and ZFS tensors, PBE0 DFT method for hyperfine coupling) level with a

QZVPP*/QZVPP basis set, which will be used in the following discussion. A semi-quantitative agreement with all the experimentally distinct ^{1}H as well as ^{13}C shifts is reached, enabling an unambiguous assignment of the experimental resonances. Indeed, the computations strongly suggest that the experimental assignments of the equally abundant C=O and CH_3 ^{13}C signals should be interchanged as compared to the previous assignment[31]. In general, the overall agreement with experiment appears to be slightly better for the entirely optimized than for the hydrogen-optimized geometry. Thus, we will focus on this model in the following. As a side note, there is as a very large difference between some of the isotropic chemical shifts calculated with B3LYP and PBE0-D3 -optimized structures (Table S9). The proton shift of particularly in the ammonia ligand exhibit large variations due to the concomitant change in the Ni-N bond length (2.145 Å with B3LYP to 2.108 Å in PBE0-D3), whereas only a small increase in the shift is seen for the methyl group, which slightly improves the agreement with experiment. In the case of carbon shifts, a large difference is found for the C=O group, whereby the agreement with experiment improves. However, none of these changes due to the structure optimization method affect the signal assignment.

Besides approximations in the electronic structure calculations (such as basis set, limited electron correlation treatment, and omission of any scalar relativistic effects presently), both intramolecular dynamics and intermolecular interaction effects are omitted from the present modeling. Therefore, quantitative agreement with experiment cannot be expected.

The total ^{13}C chemical shift tensor (Table 4) and the contribution of each of the ten physical contributions to the isotropic ^{1}H and ^{13}C shifts are presented for *trans*-[$Ni(acac)_2(NH_3)_2$], Figure 4, illustrates this assignment approach. Figure 4 clearly shows that the two major contributions originate from the orbital (δ_{orb}) and first term (contact shifts). The only other non-negligible contribution to the isotropic shift is from the sixth term, a contact-type term arising from the isotropic *g*-shift, but this is an order of magnitude smaller than the contact shift, *c.f.*, Figure 4 and

Table 4. Further insight is obtained by looking at the singly occupied orbitals (SOMO), which contribute to the hyperfine interaction and reflect the direct contribution of unpaired electron spin density (in the classical term). The ^{13}C nuclei in the carbonyl group are located in the nodal plane of this direct contribution. The total spin-density (including the indirect spin-polarization contribution) is largest (and positive) for the CH_3, as illustrated in Figure 5. This explains the much larger ^{13}C shifts observed for the CH_3 group than for C=O.

Further information is obtained by comparison of the experimentally determined and calculated principal components of the total ^{13}C chemical shift tensor in Table 4. Again a good, unambiguous agreement between the experimental and calculated ^{13}C anisotropies is obtained, where the C=O has a significantly larger anisotropy than CH, *c.f.*, Table 4. For the CH_3 group a d = -244 ppm (≈ 35 kHz at current field) is predicted, which is comparable to the spinning speeds (18-22 kHz) employed.

Similarly, calculations performed for $[Ni(acac)_2(H_2O)_2]$ *in vacuo* and compared to the experimental ^{13}C NMR data again suggest reassignment of the C=O and CH_3 resonances (Tables S2, S3, and S4).

4.3 Computationally assisted assignment of ^{13}C MAS NMR spectra of $[Ni(acac)_2(PMe_2Ph)_2]$.

We previously reported ^{13}C shifts for three phosphine complexes *trans*-$[Ni(acac)_2(L)_2]$ with L = PMe_2Ph, $PMePh_2$, and ethylene bis-diphenylphosphine (dppe)[31], and will in the following consider *trans*-$[Ni(acac)_2(PMe_2Ph)_2]$. ^{13}C shifts were obtained for NEVPT2/PBE0 calculations with the TZVP*/TZVP basis and geometry optimization of all atomic positions ("All-OPT"), as this provides the best agreement with experimental data, as discussed above (Further details in the Supporting Information). The calculated $\delta(^{13}C)$ values are presented in Table 2 and in the Supporting Information (Tables S5 and S7). We report the average for each group of chemically equivalent nuclei. E.g., C_2 and C_5 (Figure 2b), since the experimental ^{13}C MAS NMR spectra

cannot distinguish between them. The ^{13}C resonances due to the acac-ligand were assigned based on similarity with the other Ni(II) complexes investigated as discussed above. The remaining resonances with $\delta(^{13}C)$ = 68(1), 84(1), 141(1), 168(1), 239(1), 271(1), and 431(1) ppm belong to the phosphine ligands. P-C_1 and $C_{2,6}$ are computed at 596 and 353 ppm, which allows for the assignment of these resonances. In contrast, fairly large variations are seen for $C_{3,5}$ and C_4 between the two geometry-optimized structures (Table S5). Moreover, these shift are similar to P-Me, which prevents further assignment of the ^{13}C resonances except that $\delta(^{13}C)$ = 68(1), 84(1), 141(1) and 168(1) must belong to P-Me, $C_{3,5,}$ and C_4. Comparison of the ^{13}C SSNMR data for the closely related $[Ni(acac)_2(PMePh_2)_2]$ and $[Ni(acac)_2(dppe)]$[31] suggests that the sites at $\delta(^{13}C)$ = 68(1) and 84(1) may be assigned to $C_{3,5}$. Thus, it is clear that ^{13}C resonances, which experience substantial paramagnetic shifts, *e.g.,* CH_3, P-C_1, and $C_{2,6}$ can be computationally assigned and further insight can be obtained from comparison of the ^{13}C MAS NMR spectra of structurally related complexes.

4.4 Assignment of the ^1H and ^2H MAS NMR spectra of $[Ni(acac)_2(ND_3)_2]$

The experimental ^2H MAS NMR spectrum of pure *trans*-$[Ni(acac)_2(ND_3)_2]$ (Sample B) is illustrated in Figure 6a, where the resonances from a deuterated methine (CD)[31, 41] and Ni-ND_3 at $\delta(^2H)$ = -11(1) and -113(2) ppm, respectively [31]. Assignment and identification of the ^1H shifts of the methyl groups was possible by comparison of ^1H MAS NMR spectra of *trans*-$[Ni(II)(acac)_2(NH_3)_2]$ with the deuterated analogue, *c.f.*, Figure S8 and Table 5. The methine (CH) signal was also observed in the ^1H MAS NMR spectra whereas the signal of the protons in NH_3 ligands is broadened beyond detection, reflecting a large spin density on these hydrogens, *c.f.*, Figure 5. Computational results provide the following values: $\delta(^1H)$ = -189 to -167, -13 to -14, and -7 to 5 ppm for the NH_3, CH, and CH_3 groups, respectively, where the ranges result from the three geometries employed (Table 3) allowing for an unambiguous assignment of the $^{1,2}H$ resonances in

good agreement with the experimentally observed values. The largest deviation is observed for the ammonia groups involved in hydrogen bonding where the intermolecular and closest intramolecular N-H--N distances are 2.7 and 3.7 Å, respectively. They are therefore the least precisely predicted by our *in vacuo* modelling. Similarly, it was possible to assign the ^{1}H resonances from the methyl and methine protons in *trans*-[Ni(II)(acac)$_2$(H$_2$O)$_2$]H$_2$O. However, very large deviations between the experimental and calculated values are observed for the directly coordinated water protons (Ni-OH$_2$). This very likely reflects the extensive hydrogen network formed between the Ni-OH$_2$ groups and the disordered crystallographic water molecules, which cannot be reproduced by our *in vacuo* calculations.

Our first *trans*-[Ni(acac)$_2$(ND$_3$)$_2$] (sample A) was pure according to PXRD, but is nitrogen deficient (elemental analysis) and ca 20 % of a second phase according to ^{13}C MAS NMR spectrum (Figure 1). The ^{2}H MAS NMR spectrum contains three sites with $\delta(^{2}H)$ = -11(1), -113(2), and -143(2) ppm, of which the two first match *trans*-[Ni(acac)$_2$(ND$_3$)$_2$], *c.f.*, Figure 6. Two possible candidate structures are *trans*-[Ni(II)(acac)$_2$(ND$_3$)], an intermediate in the solid-gas [Ni(II)(acac)$_2$] + ND$_3$ reaction, and a *trans*-[Ni(II)(acac)$_2$(H$_2$O)(NH$_3$)], which may be present because the starting material had not been completely dehydrated First principles calculations suggest that the latter is formed (See supplementary material for a detailed discussion).

5. Conclusions

Solid-state ^{1}H and ^{13}C MAS NMR spectra for a series of paramagnetic [Ni(II)(acac)$_2$L$_2$] complexes with L = NH$_3$, ND$_3$, H$_2$O, D$_2$O, and PMe$_2$Ph were reliably assigned aided by paramagnetic shielding calculations, where *ab initio* methodology for the *g*- and zero-field splitting tensors were combined with hybrid DFT methods applied for orbital shielding and hyperfine coupling tensors. The computational approach provided detailed insight into the ten different terms, that may

contribute to the total shielding tensor. Our results demonstrate that both the directly measurable isotropic shifts, as well as the total anisotropy can be used for reliable assignment of ^{1,2}H and ^{13}C MAS NMR spectra of paramagnetic transition metal compounds.

SSNMR in combination with first principles computations is a promising method for studies of paramagnetic systems although further developments is needed to study the extended network of paramagnetic ions commonly found in inorganic materials.

6. Acknowledgements:

The authors are grateful for financial support from the Villum Foundation via the "Villum Young Investigator Program" grant VKR022364 (UGN, VBJ, NDJ, and SSNMR equipment) and 600 MHz NMR (Villum Center for Bioanalytical Services). The research leading to these results has received funding from the People Programme (Marie Curie Actions) of the European Union's Seventh Framework Program FP7 (2007-2013) under REA grant agreement n. 317127 (SAR, JV) and the Academy of Finland projects 258565 and 296292 (SAR, JM, JV). Computational resources were partially provided by CSC-IT Center for Science (Espoo, Finland) and the Finnish Grid Initiative project.

7. Supplementary Material.

Powder X-ray diffractograms, detailed description of the computational methods, additional computational results, IR spectra, and ^{1}H MAS NMR spectra are available as supporting information.

References:

[1] J. Clark Stewart, D. Segall Matthew, J. Pickard Chris, J. Hasnip Phil, I.J. Probert Matt, K. Refson, C. Payne Mike, First principles methods using CASTEP, Z. Kristal. - Crystalline Materials 220 (2005) 567.

[2] J.R. Yates, J. Pickard Chris, Computations of Magnetic Resonance Parameters for Crystalline Systems: Principles, Encl. Magn. Reson., 2009.

[3] C.J. Pickard, F. Mauri, All-electron magnetic response with pseudopotentials: NMR chemical shifts, Phys. Rev. B 63 (2001) 245101.

[4] T. Charpentier, The PAW/GIPAW approach for computing NMR parameters: A new dimension added to NMR study of solids, Solid State Nucl. Magn. Reson. 40 (2011) 1-20.

[5] S.E. Ashbrook, D. McKay, Combining solid-state NMR spectroscopy with first-principles calculations - a guide to NMR crystallography, Chem. Commun. 52. (2016) 7186-7204.

[6] Y. Ishii, N.P. Wickramasinghe, S. Chimon, A New Approach in 1D and 2D ^{13}C High-Resolution Solid-State NMR Spectroscopy of Paramagnetic Organometallic Complexes by Very Fast Magic-Angle Spinning, J. Am. Chem. Soc. 125 (2003) 3438-3439.

[7] N.P. Wickramasinghe, M. Shaibat, Y. Ishii, Enhanced sensitivity and resolution in H-1 solid-state NMR spectroscopy of paramagnetic complexes under very fast magic angle spinning, J. Am. Chem. Soc. 127 (2005) 5796-5797.

[8] N.P. Wickramasinghe, M.A. Shaibat, C.R. Jones, L.B. Casabianca, A.C. de Dios, J.S. Harwood, Y. Ishii, Progress in C-13 and H-1 solid-state nuclear magnetic resonance

for paramagnetic systems under very fast magic angle spinning, J. Chem. Phys. 128(5) (2008) 052210.

[9] Y. Nishiyama, Fast magic-angle sample spinning solid-state NMR at 60–100 kHz for natural abundance samples, Solid State Nucl. Magn. Reson. 78 (2016) 24-36.

[10] B.J. Walder, K.K. Dey, M.C. Davis, J.H. Baltisberger, P.J. Grandinetti, Two-dimensional NMR measurement and point dipole model prediction of paramagnetic shift tensors in solids, J. Chem. Phys. 142 (2015) 014201.

[11] S. Antonijevic, S. Wimperis, Separation of quadrupolar and chemical/paramagnetic shift interactions in two-dimensional ^{2}H (I = 1) nuclear magnetic resonance spectroscopy, J. Chem. Phys. 122(4) (2005) 044312-14.

[12] T. Iijima, T. Shimizu, K. Nishimura, 2H NMR pure-quadrupole spectra for paramagnetic solids, J. Magn. Reson. 251 (2015) 57-64.

[13] G. Kervern, G. Pintacuda, L. Emsley, Fast adiabatic pulses for solid-state NMR of paramagnetic systems, Chem. Phys. Lett. 435 (2007) 157-162.

[14] G. Kervern, G. Pintacuda, Y. Zhang, E. Oldfield, C. Roukoss, E. Kuntz, E. Herdtweck, J.-M. Basset, S. Cadars, A. Lesage, C. Copéret, L. Emsley, Solid-State NMR of a Paramagnetic DIAD-FeII Catalyst: Sensitivity, Resolution Enhancement, and Structure-Based Assignments, J. Am. Chem. Soc. 128 (2006) 13545-13552.

[15] R.J. Clément, A.J. Pell, D.S. Middlemiss, F.C. Strobridge, J.K. Miller, M.S. Whittingham, L. Emsley, C.P. Grey, G. Pintacuda, Spin-Transfer Pathways in Paramagnetic Lithium Transition-Metal Phosphates from Combined Broadband Isotropic Solid-State MAS NMR Spectroscopy and DFT Calculations, J. Am. Chem. Soc.134 (2012) 17178-17185.

[16] T.O. Pennanen, J. Vaara, Nuclear magnetic resonance chemical shift in an arbitrary electronic spin state, Phys. Rev. Lett. 100(13) (2008) 133002-1 - 133002-4.

[17] S.A. Rouf, J. Mareš, J. Vaara, 1H Chemical Shifts in Paramagnetic Co(II) Pyrazolylborate Complexes: A First-Principles Study, J. Chem. Theory Comp. 11 (2015) 1683-1691.

[18] A. Soncini, W. Van den Heuvel, Communication: Paramagnetic NMR chemical shift in a spin state subject to zero-field splitting, J. Chem. Phys. 138 (2013) 021103.

[19] W. Van den Heuvel, A. Soncini, NMR Chemical Shift in an Electronic State with Arbitrary Degeneracy, Phys. Rev. Lett. 109 (2012) 073001.

[20] W. Van den Heuvel, A. Soncini, NMR chemical shift as analytical derivative of the Helmholtz free energy, J. Chem. Phys. 138 (2013) 054113.

[21] J. Vaara, S.A. Rouf, J. Mareš, Magnetic Couplings in the Chemical Shift of Paramagnetic NMR, . Chem. Theory Comp. 11 (2015) 4840-4849.

[22] B. Martin, J. Autschbach, Temperature dependence of contact and dipolar NMR chemical shifts in paramagnetic molecules, J. Chem. Phys. 142 (2015) 054108.

[23] P. Hrobárik, R. Reviakine, A.V. Arbuznikov, O.L. Malkina, V.G. Malkin, F.H. Köhler, M. Kaupp, Density functional calculations of NMR shielding tensors for paramagnetic systems with arbitrary spin multiplicity: Validation on 3d metallocenes, J. Chem. Phys. 126 (2007) 024107.

[24] S. Komorovsky, M. Repisky, K. Ruud, O.L. Malkina, V.G. Malkin, Four-Component Relativistic Density Functional Theory Calculations of NMR Shielding Tensors for Paramagnetic Systems, J. Phys. Chem. A 117 (2013) 14209-14219.

[25] F. Gendron, K. Sharkas, J. Autschbach, Calculating NMR Chemical Shifts for Paramagnetic Metal Complexes from First-Principles, J. Phys. Chem. Lett. 6 (2015) 2183-2188.

[26] C.P. Grey, N. Dupre, NMR Studies of Cathode Materials for Lithium-Ion Rechargeable Batteries, Chem. Rev. 104(10) (2004) 4493-4512.

[27] C.P. Grey, Y.J. Lee, Lithium MAS NMR studies of cathode materials for lithium-ion batteries, Solid State Sci. 5 (2003) 883-894.

[28] J. Kim, D.S. Middlemiss, N.A. Chernova, B.Y.X. Zhu, C. Masquelier, C.P. Grey, Linking Local Environments and Hyperfine Shifts: A Combined Experimental and Theoretical 31P and 7Li Solid-State NMR Study of Paramagnetic Fe(III) Phosphates, J. Am. Chem. Soc. 132 (2010) 16825-16840.

[29] U.G. Nielsen, J. Majzlan, C.P. Grey, Determination and Quantification of the Local Environments in Stoichiometric and Defect Jarosite by Solid-State 2H NMR Spectroscopy, Chem. Mater. 20 (2008) 2234-2241.

[30] F.B. Johansson, A.D. Bond, U.G. Nielsen, B. Moubaraki, K.S. Murray, K.J. Berry, J.A. Larrabee, C.J. McKenzie, Dicobalt II-II, II-III, and III-III complexes as spectroscopic models for dicobalt enzyme active sites, Inorg. Chem. 47 (2008) 5079-5092.

[31] A. Lennartson, L.U. Christensen, C.J. McKenzie, U.G. Nielsen, Solid State C-13 and H-2 NMR Investigations of Paramagnetic Ni(II)(acac)(2)L-2 Complexes, Inorg. Chem. 53 (2014) 399-408.

[32] P.M. Aguiar, M.J. Katz, D.B. Leznoff, S. Kroeker, Natural abundance 13C and 15N solid-state NMR analysis of paramagnetic transition-metal cyanide coordination polymers, Phys. Chem. Chem. Phys. 11 (2009) 6925-6934.

[33] A. Flambard, F.H. Köhler, R. Lescouëzec, Revisiting Prussian Blue Analogues with Solid-State MAS NMR Spectroscopy: Spin Density and Local Structure in $[Cd_3\{Fe(CN)_6\}_2]\cdot 15\,H_2O$, Ang. Chem. Int. Ed. 48 (2009) 1673-1676.

[34] L. Ouyang, P.M. Aguiar, R.J. Batchelor, S. Kroeker, D.B. Leznoff, A paramagnetic Cu(I)/Cu(II)/Zn(II) coordination polymer with multiple CN-binding modes and its solid-state NMR characterization, Chem. Commun. (2006) 744-746.

[35] M.I.H. Mohideen, B. Xiao, P.S. Wheatley, A.C. McKinlay, Y. Li, A.M.Z. Slawin, D.W. Aldous, N.F. Cessford, T. Düren, X. Zhao, R. Gill, K.M. Thomas, J.M. Griffin, S.E. Ashbrook, R.E. Morris, Protecting group and switchable pore-discriminating adsorption properties of a hydrophilic–hydrophobic metal–organic framework, Nat. Chem. 3 (2011) 304-310.

[36] M. Bühl, S.E. Ashbrook, D.M. Dawson, R.A. Doyle, P. Hrobárik, M. Kaupp, I.A. Smellie, Paramagnetic NMR of Phenolic Oxime Copper Complexes: A Joint Experimental and Density Functional Study, Chem.- Eur. J. 22(2016) 15328-15339.

[37] X. Kong, V.V. Terskikh, R.L. Khade, L. Yang, A. Rorick, Y. Zhang, P. He, Y. Huang, G. Wu, Solid-State ^{17}O NMR Spectroscopy of Paramagnetic Coordination Compounds, Ang. Chem. Int. Ed. 54 (2015) 4753-4757.

[38] D.M. Dawson, L.E. Jamieson, M.I.H. Mohideen, A.C. McKinlay, I.A. Smellie, R. Cadou, N.S. Keddie, R.E. Morris, S.E. Ashbrook, High-resolution solid-state 13C NMR spectroscopy of the paramagnetic metal-organic frameworks, STAM-1 and HKUST-1, Phys. Chem. Chem. Phy. 15 (2013) 919-929.

[39] A. Nayeem, J.P. Yesinowski, Calculation of magic-angle spinning nuclear magnetic resonance spectra of paramagnetic solids, J. Chem. Phys. 89 (1988) 4600-4608.

[40] H. Lee, T. Polenova, R.H. Beer, A.E. McDermott, Lineshape fitting of deuterium magic angle shinning spectra of paramagnetic compounds in slow and fast limit motion regimes, J. Am. Chem. Soc. 121 (1999) 6884-6894.

[41] K. Liu, D. Ryan, K. Nakanishi, A. McDermott, Solid State NMR Studies of Paramagnetic Coordination Complexes: A Comparison of Protons and Deuterons in Detection and Decoupling, J. Am. Chem. Soc. 117 (1995) 6897-6906.

[42] R.J. Kurland, B.R. McGarvey, Isotropic NMR shifts in transition metal complexes: The calculation of the fermi contact and pseudocontact terms, J. Magn. Reson. (1969) 286-301.

[43] A. Kubica, J. Kowalewski, D. Kruk, M. Odelius, Zero-field splitting in nickel(II) complexes: A comparison of DFT and multi-configurational wavefunction calculations, J. Chem. Phys. 138. (2013) 064304.

[44] B. Roos, A new method for large-scale Cl calculations, Chem. Phys. Lett. 15 (1972) 153-159.

[45] C. Angeli, S. Borini, R. Cimiraglia, An application of second-order n-electron valence state perturbation theory to the calculation of excited states, Theor. Chem. Acc. 111(2-6) (2004) 352-357.

[46] H.M. McConnell, D.B. Chesnut, Theory of Isotropic Hyperfine Interactions in π-Electron Radicals, J. Chem. Phys. 28. (1958) 107-117.

[47] M. Kaupp, F.H. Köhler, Combining NMR spectroscopy and quantum chemistry as tools to quantify spin density distributions in molecular magnetic compounds, Coord. Chem. Rev. 253 (2009) 2376-2386.

[48] L. Benda, J. Mareš, E. Ravera, G. Parigi, C. Luchinat, M. Kaupp, J. Vaara, Pseudo-Contact NMR Shifts over the Paramagnetic Metalloprotein CoMMP-12 from First Principles, Ang. Chem. Int. Ed. 55 (2016) 14713-14717.

[49] J. Vaara, Chapter 3 - Chemical Shift in Paramagnetic Systems, in: H.C. Rubén (Ed.), Science and Technology of Atomic, Molecular, Condensed Matter & Biological Systems, Elsevier2013, pp. 41-67.

[50] J. Autschbach, Chapter One - NMR Calculations for Paramagnetic Molecules and Metal Complexes, in: A.D. David (Ed.), Ann. Rep. Comp. Chem., Elsevier 2015, pp. 3-36.

[51] S.K. Kumara Swamy, A. Karczmarska, M. Makowska-Janusik, A. Kassiba, J. Dittmer, Solid-State NMR Correlation Experiments and Distance Measurements in Paramagnetic Metalorganics Exemplified by Cu-Cyclam, Chem. Phys. Chem. 14 (2013) 1864-1870.

[52] M.J.T. Frisch, G. W.; Schlegel, H. B.; Scuseria, G. E.; Robb, M. A.; Cheeseman, J. R.; Scalmani, G.; Barone, V.; Mennucci, B.; Petersson, G. A.; Nakatsuji, H.; Caricato, M.; Li, X.; Hratchian, H. P.; Izmaylov, A. F.; Bloino, J.; Zheng, G.; Sonnenberg, J. L.; Hada, M.; Ehara, M.; Toyota, K.; Fukuda, R.; Hasegawa, J.; Ishida, M.; Nakajima, T.; Honda, Y.; Kitao, O.; Nakai, H.; Vreven, T.; MontgomeryJ. A.; Peralta, J. E.; Ogliaro, F.; Bearpark, M.; Heyd, J. J.; Brothers, E.; Kudin, K. N.; Staroverov, V. N.; Kobayashi, R.; Normand, J.; Raghavachari, K.; Rendell, A.; Burant, J. C.; Iyengar, S. S.; Tomasi, J.; Cossi, M.; Rega, N.; Millam, J. M.; Klene, M.; Knox, J. E.; Cross, J. B.; Bakken, V.; Adamo, C.; Jaramillo, J.; Gomperts, R.; Stratmann, R. E.; Yazyev, O.; Austin, A. J.; Cammi, R.; Pomelli, C.; Ochterski, J. W.; Martin, R. L.; Morokuma, K.; Zakrzewski, V. G.; Voth, G. A.; Salvador, P.; Dannenberg, J. J.; Dapprich, S.;

Daniels, A. D.; Farkas, O.; Foresman, J. B.; Ortiz, J. V.; Cioslowski, J.; Fox, D. J. Gaussian, Inc., Wallingford CT, 2009., Gaussian 09, 2009.

[53] F. Neese, Orca, an ab Initio, Density Functional and Semiempirical Program Package, Version 3.0.1, 2012.

[54] J.P. Perdew, K. Burke, M. Ernzerhof, Generalized Gradient Approximation Made Simple, Phys. Rev. Lett. 77 (1996) 3865-3868.

[55] J.P. Perdew, K. Burke, M. Ernzerhof, Generalized Gradient Approximation Made Simple, Phys. Rev. Lett. 78(7) (1997) 1396-1396.

[56] C. Adamo, V. Barone, Toward reliable density functional methods without adjustable parameters: The PBE0 model, The Journal of Chemical Physics 110(13) (1999) 6158-6170.

[57] (TURBOMOLE V6.5 2013), a development of (University of Karlsruhe) and (Forschungszentrum Karlsruhe GmbH), 1989-2007, (TURBOMOLE GmbH), since 2007; available from (http://www.turbomole.com), 2013.

[58] A.D. Becke, Density-functional thermochemistry. III. The role of exact exchange, The J. Chem. Phys. 98 (1993) 5648-5652.

[59] C. Lee, W. Yang, R.G. Parr, Development of the Colle-Salvetti correlation-energy formula into a functional of the electron density, Phys. Rev. B 37 (1988) 785-789.

[60] P.J. Stephens, F.J. Devlin, C.F. Chabalowski, M.J. Frisch, Ab Initio Calculation of Vibrational Absorption and Circular Dichroism Spectra Using Density Functional Force Fields, J. Phys. Chem. 98 (1994) 11623-11627.

[61] F. Weigend, Accurate Coulomb-fitting basis sets for H to Rn, Phys. Chem. Chemical Phys. 8 (2006) 1057-1065.

[62] F. Weigend, R. Ahlrichs, Balanced basis sets of split valence, triple zeta valence and quadruple zeta valence quality for H to Rn: Design and assessment of accuracy, Phys. Chem. Chem. Phys. 7 (2005) 3297-3305.

[63] S. Grimme, J. Antony, S. Ehrlich, H. Krieg, A consistent and accurate ab initio parametrization of density functional dispersion correction (DFT-D) for the 94 elements H-Pu, J. Chem.l Phys. 132 (2010) 154104.

[64] D.B. Chesnut, K.D. Moore, Locally dense basis sets for chemical shift calculations, J. Comp. Chem. 10 (1989) 648-659.

[65] G.A. DiLabio, D.A. Pratt, A.D. LoFaro, J.S. Wright, Theoretical Study of X−H Bond Energetics (X = C, N, O, S): Application to Substituent Effects, Gas Phase Acidities, and Redox Potentials, J. Phys. Chem. A 103(11) (1999) 1653-1661.

[66] H. Jensen, M.S. Gordon, SPLICING-I - using mixed basis-set in abinitio calculations J. Comp. Chem. 12(4) (1991) 421-426.

[67] N.P. Wickramasinghe, M. Kotecha, A. Samoson, J. Past, Y. Ishii, Sensitivity enhancement in C-13 solid-state NMR of protein microcrystals by use of paramagnetic metal ions for optimizing H-1 T-1 relaxation, J. Magn. Reson. 184 (2007) 350-356.

Figures and Tables

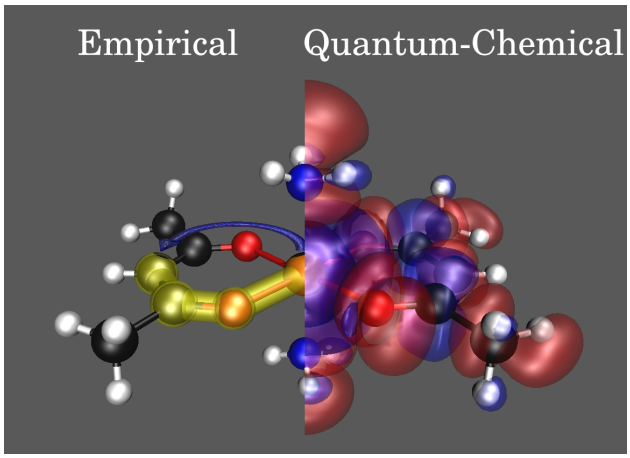

Figure 1. The paramagnetic interactions from the empirical point-of-view (left) and quantum chemistry (right) illustrated for [Ni(II)$(acac)_2(NH_3)_2$]. The contact shift (yellow) and dipolar (blue) interactions, which are mediated through the chemical bonds and through-space dipolar interaction, respectively, are illustrated for ^{13}C in the methine group (CH). The right-hand-side shows the unpaired electron spin density on all carbons (see discussion in the text), which gives rise to the nine genuinely paramagnetic shielding contributions.

a)

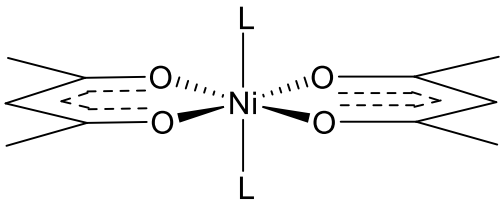

L=H_2O, D_2O, NH_3, ND_3 and PMe_2Ph

b)

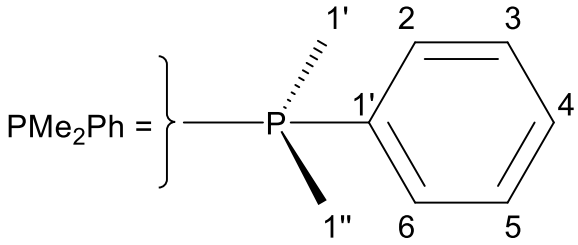

Figure 2. a) The molecular structure of the [Ni(II)$(acac)_2L_2$] complexes investigated with L = NH_3, ND_3, H_2O, D_2O, and PMe_2Ph. b) The labelling of the carbon atoms in the dimethyl phenyl phosphine ligand (PMe_2Ph).

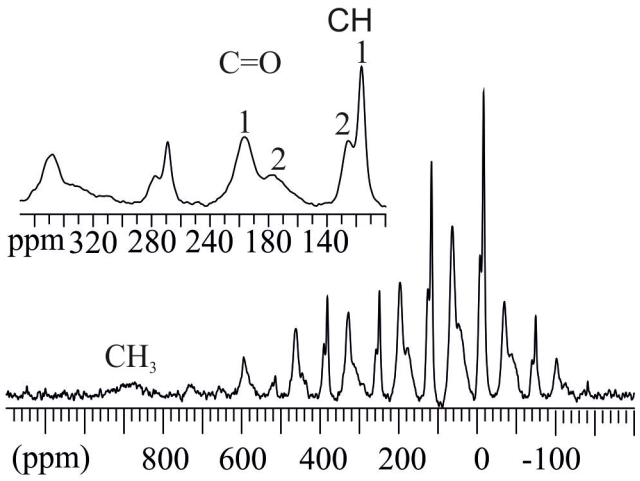

Figure 3: ^{13}C MAS NMR spectrum of $[Ni(acac)_2(ND_3)_2]$ (Method B) with the isotropic resonances indicated in the inset (top left): 1 and 2 correspond to the isotropic ^{13}C resonances from $[Ni(acac)_2(ND_3)_2]$[31] and impurity, respectively (see discussion in text).

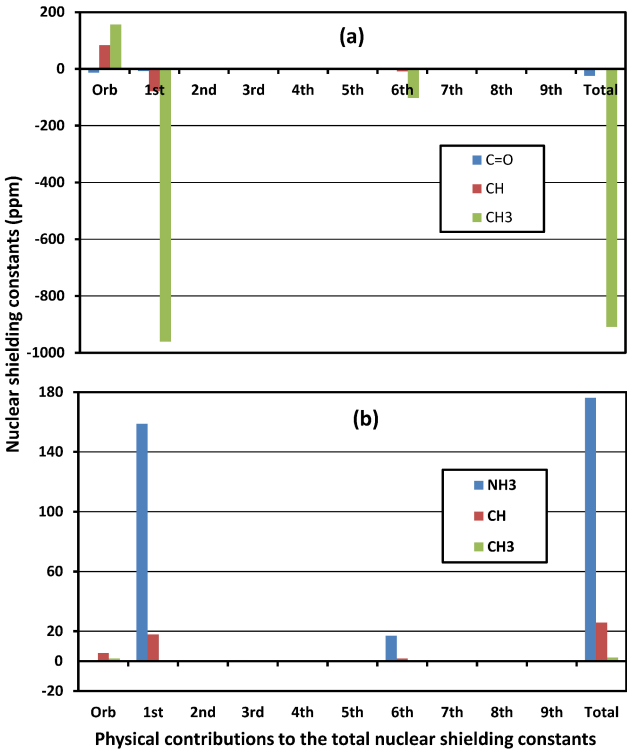

Figure 4. Calculated isotropic shielding for a) ^{13}C and b) ^{1}H illustrating the contribution from the orbital (σ_{orb}, orbital shielding) and each of the nine components of the paramagnetic shielding tensor (Table 1). The two significant contributions to the paramagnetic shielding are the terms 1 (Fermi contact shift, δ_{con}) and 6 (contact with isotropic *g*-shift).

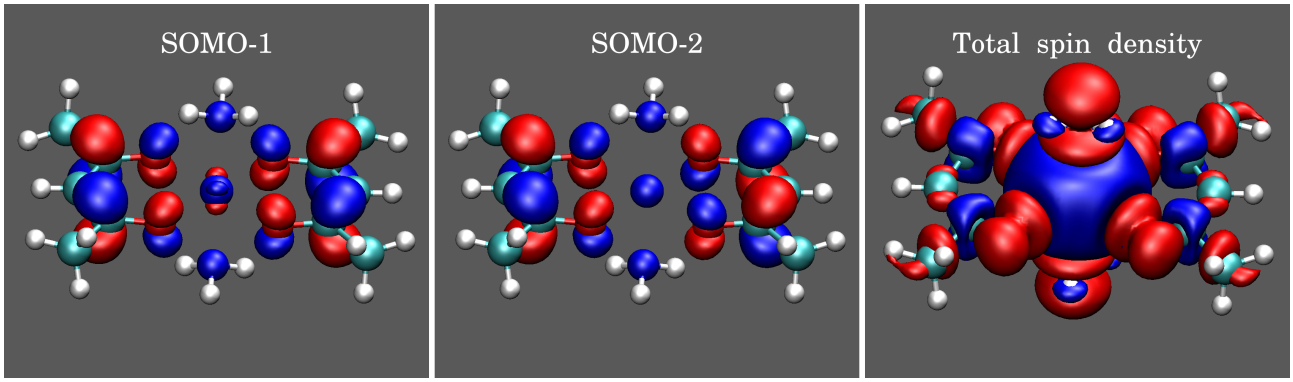

Figure 5. The two singly-occupied orbitals (SOMO-1 and SOMO-2), where the unpaired electrons are located as well as the total spin density, which includes spin polarization contributions, with positive and negative spin densities shown in red and blue, respectively.

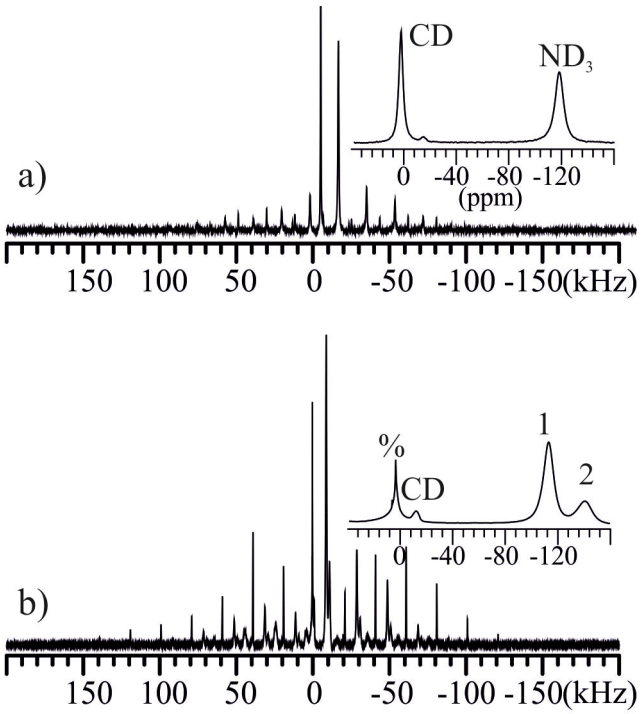

Figure 6. The ^{2}H MAS NMR spectrum of the samples of *trans*-[Ni(II)$(acac)_2(ND_3)_2$] prepared by a) method A and b) B respectively. The isotropic resonances for the different sites are indicated in the inset: Methine of the D_1-acac ligand (CD), the ammonia ligand directly coordinated to Ni- (ND_3), of which the larger (1) resonance originates from [Ni(II)$(acac)_2(ND_3)_2$] and the smaller (2) most likely from [Ni(II)$(acac)_2(ND_3)(D_2O)$] .% indicates surface water and/or ammonia.

Table 1. The relationship between the quantum-chemical terms (Ref.[16, 17, 21]) and the experimentally determined NMR parameters for paramagnetic systems.[a]

Term	Theory / equation	Origin[b]	(SS)NMR Observable[c]	Rank
orb	σ_{orb}	orbital interactions	chemical shift tensor	0,1,2
1st	$g_e A_{con} <S_\varepsilon S_\tau>$	NR contact HFC	term in contact shift	0,2
2nd	$g_e \Sigma_b A_{b\tau}^{dip} <S_\varepsilon S_\tau>$	NR dipolar HFC	term in dipolar shift	0,1,2
3rd	$g_e A_{PC} <S_\varepsilon S_\tau>$	isotropic SO correction to HFC	term in contact shift	0,2
4th	$g_e \Sigma_b A_{b\tau}^{dip,2} <S_\varepsilon S_b>$	rank-2 SO correction to HFC	term in dipolar shift	0,1,2
5th	$g_e \Sigma_b A_{b\tau}^{as} <S_\varepsilon S_b>$	rank-1 SO correction to HFC	correction to tensor anisotropy	1,2
6th	$\Delta g_{iso} A_{con} <S_\varepsilon S_\tau>$	isotropic SO correction to g	term in contact shift	0,2
7th	$\Delta g_{iso} \Sigma_b A_{b\tau}^{dip} <S_\varepsilon S_b>$	isotropic SO correction to g	term in dipolar shift	0,1,2
8th	$A_{con} \Sigma_a \Delta\tilde{g}_{\varepsilon a} <S_a S_\tau>$	anisotropic SO correction to $\boldsymbol{g}$	anisotropic contact shift	0,1,2
9th	$\Sigma_{ab} \Delta\tilde{g}_{\varepsilon a} A_{b\tau}^{dip} <S_a S_b>$	anisotropic SO correction to $\boldsymbol{g}$	pseudocontact shift	0,1,2
Total[d]	$\boldsymbol{\sigma}_{\mathrm{orb}} - \frac{\mu_B}{\gamma\hbar kT} \boldsymbol{g} \cdot \langle \boldsymbol{SS} \rangle \cdot \boldsymbol{A}$		total shift	0,1,2

[a]The chemical shift ($\delta_{CSA} = \sigma_{ref} - \sigma_{orb}$). The hyperfine shift contributions are obtained from terms 1-9 as $\delta_{con} = -\sigma_{con}$ etc. [b]The Cartesian coordinate indices $\varepsilon, \tau = x, y, z$ are used to indicate the tensorial component $\sigma_{\varepsilon\tau}$ to which the terms contribute to. The indices $a, b = x, y, z$ are summed over. [c]NR = nonrelativistic, HFC = hyperfine coupling, SO = spin-orbit, g = isotropic g-factor, $\boldsymbol{g}$ = g-tensor. [d] Note that the terms orb, 1-4, and 6-9 contribute to the isotropic shielding constant and shift in the presence of ZFS. Similarly, all the terms contribute to the rank-2 anisotropy of the shielding tensor

and, hence, the tensor eigenvalues. [e]Total shielding expression with the dyadic involving the effective spin operators $\boldsymbol{S}$ defined as $\langle S_a S_b \rangle = \frac{\sum_{nm} Q_{nm} \langle n|\boldsymbol{S}|m\rangle\langle m|\boldsymbol{S}|n\rangle}{\sum_n \exp(-E_n/kT)}$, where $|n\rangle$ and E_n are the eigenfunctions and -values of the ZFS Hamiltonian, and the symmetric matrix Q_{nm} is expressible using E_n and E_m.

Table 2. ^{13}C NMR data for *trans*-[Ni(acac)$_2$L$_2$] with L = H_2O, D_2O, NH_3, ND_3, and PMe_2Ph with previous (empirical)[31] and computationally assisted assignment (New assign).

Compound	**Previous [31]**	**Exp.[a] δ(^{13}C) (ppm)**	**Calc. δ(^{13}C)[b] (ppm)**	**T_1(ms) Exp**	**New Assign.**
Trans-[Ni(acac)$_2$(ND$_3$)$_2$]	NA	198(2)			C=O
		118(2)			CH
		885(10)			CH_3
Trans-[Ni(acac)$_2$(NH$_3$)$_2$]	CH_3	199(1)	216, 207, 216, 206	0.54(3)	C=O
	CH	119(1)	189, 191	1.24(4)	CH
	C=O	883(20)	1094,1097, 1094,1097	1.32(6)	CH_3
Trans-[Ni(acac)$_2$(H$_2$O)$_2$](H$_2$O)	CH_3	188(1)	188	1.08(12)	C=O
		201(1)	209	1.35(11)	
		245(1)	317	1.08(1)	
		311(2)	405	1.28(13)	
	CH	123(1)	208	3.1(2)	CH
		134(1)	234	2.9(2)	
	C=O	796(20)[a]	1055,1062	1.14(6)	CH_3
		891(20)[a]	1220,1247	0.91(8)	
Trans-[Ni(acac)$_2$(D$_2$O)$_2$](D$_2$O)	CH_3	188(1)		1.08(9)	C=O
		200(2)		1.3(2)	
		243(2)		1.1(2)	
		305(2)		1.0(1)	
	CH	123(1)		3.1(2)	CH
		134(1)		2.9(2)	
	C=O	796(20)[a]		1.14(6)	CH_3
		891(20)[a]		0.91(8)	
Trans-[Ni(acac)$_2$(PMe$_2$Ph)$_2$]	$C_{2,6}$	68(1),	58 (P-Me)		$C_{3,5}$?
	$C_{2,6}$	84(1)	118 ($C_{3,5}$)		$C_{3,5}$?
	C_4	141(2)	199 (C_4)		
	$C_{3,5}$	168(1)			
	CH	131(2)	124		CH
	CH_3	207(1)	277		C=O
	CH_3	220(1)	277		C=O
	$C_{3,5}$	239(1)	353		$C_{2,6}$
	C_1	271(1)	353		$C_{2,6}$
	P-CH_3	431(1)	597		C_1
	C=O	950(30)	1142		CH_3

[a] Reassigned from the previous work[31] [b] Results from calculations at the NEVPT2/PBE0 level, QZVPP*/QZVPP basis, structure with hydrogen positions optimized, except for L = PPh_2Me_2 ligands, for which a completely optimized structure (A-OPT) was used. % indicates that the parameter could not be determined experimentally (see discussion on text).

Table 3. Calculated isotropic ^{1}H and ^{13}C chemical shifts for *trans*-[$Ni(acac)_2(NH_3)_2$] at 298 K.[a]

	^{1}H			^{13}C		
Structure[b]	**NH_3**	**C-H**	**CH_3**	**C=O**	**C-H**	**CH_3**
EXP	-189.0	-13.3	-7.5	145.0	179.1	922.9
H-OPT	-174.9	-14.6	1.2	211.1	189.5	1095.5
All-OPT	-166.6	-13.8	2.8	266.5	85.2	1026.7
Exp.[c]	-113(2)	-12(2)	5(3)	198	118	883

[a] NEVPT2/PBE0 level of theory with QZVPP*/QZVPP basis set, in the notation (method for **D** and **g**/method for **A**).

[b] EXP, H-OPT, All-OPT denote the experimental X-ray geometry, the structure obtained from it via optimizing the hydrogen positions, and the entirely optimized structure, respectively.

[c] Experimental results. The assignments of the signals for nuclei have been interchanged in the present work, as compared to Ref. [31].

Table 4. Physical contributions to the calculated principal values (in ppm) of the total ^{13}C nuclear shielding tensor in *trans*-[Ni(acac)$_2$(NH$_3$)$_2$]. Calculations are at the NEVPT2/PBE0 level using a QZVPP*/QZVPP basis and the hydrogen-optimized structure. The total principal values have been ordered according to $\sigma_{11} < \sigma_{22} < \sigma_{33}$ (total shielding eigenvalues). A comparison of the experimental (Exp) and computational (Comp) values of the chemical shift tensor components [isotropic shift (δ_{iso}), asymmetry parameter (η) and anisotropy (*d*)] are given for a comparison with the experimentally determined data.

NH$_3$	**C=O**			**CH**			**CH$_3$**		
Terms[a]	σ_{11}	σ_{22}	σ_{33}	σ_{11}	σ_{22}	σ_{33}	σ_{11}	σ_{22}	σ_{33}
orb	-98	-51	110	-27	149	128	187	135	149
1st	-8	-8	-8	-79	-79	-80	-960	-963	-960
2nd	-519	134	387	-275	65	212	-245	125	120
3rd	-4	-4	-4	0	0	0	-2	-2	-2
4th	-16	-1	17	-24	13	11	-5	4	1
5th	0	0	0	0	0	0	0	0	0
6th	-1	-1	-1	-8	-8	-8	-102	-103	-103
7th	-55	14	41	-29	7	23	-26	13	13
8th	0	0	0	0	0	0	2	-3	1
9th	2	0	1	1	0	1	0	0	0
Total	**-700**	**83**	**544**	**-442**	**146**	**286**	**-1152**	**-792**	**-781**
	Comp	**Exp**		**Comp**	**Exp**		**Comp**	**Exp**	
$\delta_{\iota\sigma o}$	211	199(1)		190	119(1)		1095	883(20)	
η	0.68	0.67(5)		0.3	0.00(5)		0.04	%	
d	-675	-505(5)		-439	-353(7)		-244	%	

a The numbering of the mechanisms refers to Table 1.

% indicates that the parameter could not be determined experimentally.

Table 5: A summary of the ^{1}H and ^{2}H NMR data determined for *trans*-[$Ni(acac)_2L_2$] with L = H_2O, D_2O, NH_3, and ND_3. All values are experimentally determined except the calculated $\delta(^{1}H)$ and not determined experimentally (NA).

Compound	**Group**	**Exp. $\delta(^{1}H)$ (ppm)**	**Exp. $\delta(^{2}H)$ (ppm)**	**Calc.[a] $\delta(^{1}H)$ (ppm)**	**C_Q (kHz)**	**η_Q**
Trans-[$Ni(acac)_2(NH_3)_2$]	CH_3	5(3)	NA	1.2	NA	NA
	CH	-12(2)	-11(1)	-15	NA	NA
	Ni-NH_3	NA	-113(2)	-175	NA	NA
Trans-[$Ni(acac)_2(ND_3)_2$]	CH_3	6(3)	NA		NA	NA
	CH	-11(2)	-11(1)		160(20)	NA
	Ni-NH_3	NA	-113(2)		99(20)	NA
			-141(2)		109(20)	NA
	Unknown		60(10)[b]			
Trans-[$Ni(acac)_2(H_2O)_2$](H_2O)	CH_3	6(3)	NA[c]	-6	NA	NA
	CH	-10(2)	-11	-6	NA	NA
	Ni-H_2O	NA		-152	NA	NA
Trans-[$Ni(acac)_2(D_2O)_2$](D_2O)[d]	CH_3	8(2)	NA		NA	NA
	CH	-9(2)	-11(1)		185(2)	0.85(5)
	Ni-D_2O	NA	25(1),		115(10)	0.8(1)
			17(1),			
			6(1)			

[a] Results from calculations at the NEVPT2/PBE0 level, QZVPP*/QZVPP basis, structure with hydrogen positions optimized. [b] Two or more overlapping resonances from an unknown impurity. NA not applicable. [c] This resonance is too weak for a reliable determination. [d]Ref[31] and this work